PROGRESS IN PHOTOVOLTAICS: RESEARCH AND APPLICATIONS
Prog. Photovolt: Res. Appl. 2007; **15**:677–696
Published online in Wiley InterScience (www.interscience.wiley.com). DOI: 10.1002/pip.791

Special Issue

A Review of Charge Transport and Recombination in Polymer/Fullerene Organic Solar Cells

A. Pivrikas[1*,†], N. S. Sariciftci[1], G. Juška[2] and R. Österbacka[3]
[1]*Department of Physical Chemistry, Johannes Kepler University, Linz Institute for Organic Solar Cells (LIOS), Altenberger Strasse 69, A-4040 Linz, Austria*
[2]*Department of Solid State Electronics, Vilnius University, Saulėtekio 9 III K, 10222 Vilnius, Lithuania*
[3]*Center for Functional Materials and Department of Physics, Åbo Akademi University, Porthansgatan 3, 20500 Turku, Finland*

The charge carrier transport and recombination in two types of thermally treated bulk-heterojunction solar cells is reviewed: in regioregular poly(3-hexylthiophene) (RRP3HT) mixed with 1-(3-methoxycarbonyl)propyl-1-phenyl-[6,6]-methanofullerene (PCBM) and in the blend of poly[2-methoxy-5-(3,7-dimethyloctyloxy)-phenylene vinylene] (MDMO-PPV) mixed with PCBM. The charge carrier mobility and bimolecular recombination coefficient have been comparatively studied by using various techniques including Time-of-Flight (ToF), Charge Extraction by Linearly Increasing Voltage (CELIV), Double Injection (DI) transients, Current–Voltage (I–V) technique. It was found that the carrier mobility is at least an order of magnitude higher in RRP3HT/PCBM blends compared to MDMO-PPV/PCBM. Moreover, all used techniques demonstrate a heavily reduced charge carrier recombination in RRP3HT/PCBM films compared to Langevin-type carrier bimolecular recombination in MDMO-PPV/PCBM blends. As a result of long carrier lifetimes the formation of high carrier concentration plasma in RRP3HT/PCBM blends is demonstrated and plasma extraction methods were used to directly estimate the charge carrier mobility and bimolecular recombination coefficients simultaneously. A weak dependence of bimolecular recombination coefficient on the applied electric field and temperature demonstrates that carrier recombination is not dominated by charge carrier mobility (Langevin-type recombination) in RRP3HT/PCBM blends. Furthermore, we found from CELIV techniques that electron mobility in RRP3HT/PCBM blends is independent on relaxation time in the experimental time window (approx. hundreds of microseconds to tens of milliseconds). This reduced carrier bimolecular recombination in RRP3HT/PCBM blends implies that the much longer carrier lifetimes can be reached at the same concentrations which finally results in higher photocurrent and larger power conversion efficiency of RRP3HT/PCBM solar cells. Copyright © 2007 John Wiley & Sons, Ltd.

KEY WORDS: time-of-flight; bulk-heterojunction; solar cells; bimolecular recombination; Langevin recombination; charge transport

Received 6 July 2007

INTRODUCTION TO CHARGE CARRIER TRANSPORT IN ORGANIC SOLAR CELLS

Increasing energy consumption and rising energy prices in the world forces to look for energy alternatives, one of the most promising being the photovoltaic solar energy

*Correspondence to: A. Pivrikas, Department of Physical Chemistry, Johannes Kepler University, Linz Institute for Organic Solar Cells (LIOS), Altenberger Strasse 69, A-4040 Linz, Austria.
†E-mail: almantas.pivrikas@jku.at

conversion. Various concepts and device architectures of organic solar cells have been actively studied for more than 30 years.[1–8] Efficiencies, routinely exceeding 4–5% have been reached in thin-film organic solar cells today. From purely academic point of view, the research of organic solar cells is interesting due to novel photophysical phenomena, whereas technologically low fabrication costs due to roll-to-roll printing possibilities drive the economic point of view.

There are four main important processes which might limit the power conversion efficiency of photovoltaic devices:[9]

1. Light absorption in the film.
2. Free charge carrier generation.
3. Charge transport to the opposite electrodes and extraction by the electrodes.
4. Carrier recombination.

When the photoexcitation (an exciton) is created after the photon energy is absorbed in the material, mobile charge carriers must be created by splitting the exciton into a free electron and hole. Therefore, donor and acceptor blends are used in the organic photovoltaics to facilitate photoinduced charge transfer. If the exciton reaches the donor–acceptor interface, the electron can then be transferred to the material with lower lying Lowest Unoccupied Molecular Orbit (LUMO) if $I_{D*} - E_A - \text{Coulomb} < 0$, where I_{D*} is the ionization potential of the excited donor, E_A the electron affinity of the acceptor, and Coulomb summarizes all the electrostatic interactions including the exciton binding energy and all polarizations. The important parameters here are the exciton diffusion length and the distance between the donor and acceptor phases.

Furthermore, both these charge carriers must be transported to the opposite electrodes and reach them prior to recombination. If after photoinduced charge transfer the electron and hole are still bound by the Coulomb potential, then typically for low mobility materials, they cannot escape from each others attraction and will finally recombine. However, the excitons can be split into free electrons and holes when the carrier dissipation distance is larger than the Coulomb radius. To fulfill this condition the Coulomb field must be screened or charge carrier hopping distance must be larger than the Coulomb radius (for low mobility materials it is unrealistic).[10] In this case mobile charge carriers can be transported to the contacts either by carrier diffusion or electric field induced drift. In order to have unity quantum efficiency for charge extraction, one needs to fulfill the condition that the charge carrier transit time t_{tr} is much smaller than the carrier lifetime τ ($t_{tr} \ll \tau$). The carrier transit time $t_{tr} = d/\mu E$ is determined by the charge carrier mobility μ, sample thickness d, and the electric field E inside the film. If the photocurrent is governed by the carrier drift in the applied electric field, then the drift distance $l_{drift} = \mu\tau E$. If the photocurrent is governed by the carrier diffusion, then the diffusion distance $l_{diffusion} = \sqrt{D\tau} = \sqrt{\mu\tau kT/e}$, where D is the diffusion coefficient, k the Boltzmann constant, and e is the electron charge. As it can be seen from above in both cases the $\mu\tau$ product will determine the average distance the charge carrier can travel before recombination. The mobility-lifetime product $\mu\tau$ is therefore an important parameter determining whether or not the power conversion efficiency of the photovoltaic devices is limited by the charge transport and recombination.

In the following sections we will discuss the charge carrier mobility and lifetimes in polymer/fullerene bulk-heterojunction solar cells (in RRP3HT/PCBM and poly[2-methoxy-5-(3,7-dimethyloctyloxy)-phenylene vinylene] (MDMO-PPV)/PCBM blends) measured using Time-of-Flight (ToF), Charge Extraction by Linearly Increasing Voltage (CELIV), and Double Injection (DI) transient and plasma extraction and current–voltage (*I–V*) techniques. Results clearly show a reduced recombination in the high efficiency solar cells using regioregular poly(3-hexylthiophene) (RRP3HT)/PCBM mixtures.

High light intensity ToF

Using high pump intensity ToF we comparatively studied the extracted charge in the thermally treated RRP3HT/PCBM and MDMO-PPV/PCBM bulk-heterojunction solar cells. First, introduction to ToF and high light intensity ToF technique will be presented and later, we show the results from RRP3HT/PCBM samples and these results will be compared to measurements in MDMO-PPV/PCBM bulk-heterojunction solar cells. An analytical equation to estimate the bimolecular recombination coefficient experimentally will be shown.

Introduction to ToF technique

ToF is a well known technique and it is widely used to measure the charge carrier transport in various low mobility (and low conductivity) semiconductors. A schematic ToF circuitry, timing diagram, and charge carrier transport inside the film are shown in Figure 1.

DOI: 10.1002/pip

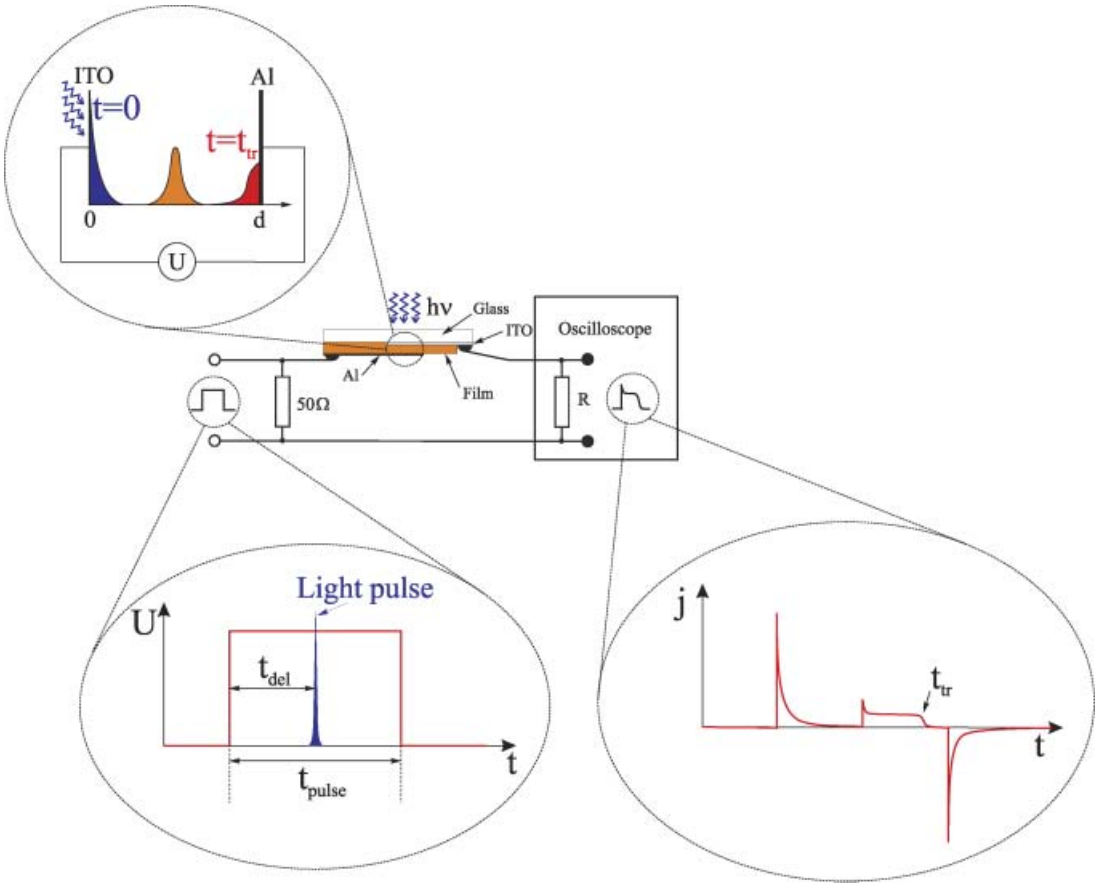

Figure 1. Typical ToF setup, where the capacitance of the sample and the load resistance R in the oscilloscope form a differentiating RC circuit. Top magnified picture shows the transport dynamics of charge carriers photogenerated at the surface of the film under applied voltage U. Bottom left picture shows the timing of light and voltage pulses and right picture shows the current transient response in the oscilloscope with the characteristic transit time t_{tr} noting the arrival of charge carriers to an opposite contact

Even though it is possible to apply ToF technique in the volume photogeneration case and in integral mode,[11] the most commonly used mode of ToF is differential low light intensity ToF with surface absorption, ensuring that a small amount of charges is generated near the transparent electrode compared to the charge stored on the contacts (CU). Thin sheet of photogenerated carriers ($\alpha d > 1$) can then be transported through the film with thickness d when an external voltage U is applied. When the packet of charge carriers reaches the opposite contact the photocurrent drops forming a characteristic feature at transit time t_{tr} as can be seen in the oscilloscope, see Figure 1. The charge carrier mobility is then calculated using the following equation: $\mu = d^2/t_{tr}U$.

Low light intensity ToF mode ensures that the externally applied electric field inside the film is disturbed only fractionally throughout the film which simplifies the interpretation of the current transients. High light intensity ToF studies are also possible[12] and moreover, they can reveal additional information about the charge carrier recombination. In this case, a high intensity laser pump is used to photogenerate a large amount of charges inside the film. A (large) reservoir of charges is created inside the film, where the amount of charge in the reservoir is much larger than the charge stored on the sample electrodes (CU) due to applied external voltage U.

In Figure 2 ideal schematic ToF transients are shown for different light intensities, where the intensity is shown in the units of photogenerated charges Q_0. Typical Small Charge Current (SCC) at low light intensity, Space Charge Perturbed Current (SCPC) at moderate intensity, and Space Charge Limited

DOI: 10.1002/pip

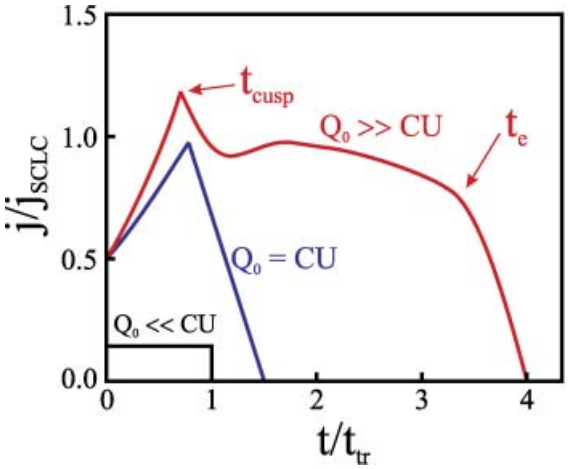

Figure 2. Ideal ToF transients without carrier recombination for different laser light intensities, demonstrating typical SCC (low light intensity, $Q_0 \ll$ CU), SCPC (moderate light intensity, $Q_0 \approx$ CU), and SCLC (high light intensity, $Q_0 \gg$ CU) current transients. The reservoir extraction time t_e (please note, that it is only present in SCLC case) is much larger than carrier transit time t_{tr} or t_{cusp}. (Reprinted figure with permission from A. Pivrikas, G. Juška, R. Österbacka, M. Westerling, M. Viliūnas, K. Arlauskas, and H. Stubb, *Physical Review B* 2005; **71**: 125205. Copyright (2005) by the American Physical Society)

Current (SCLC) at high intensity shows three cases of the current transients. In case when the amount of photogenerated charge is much larger than charge on the contacts ($Q_0 \gg$ CU) and when the charge carrier recombination in the reservoir is slow (e.g., carrier lifetime is longer than transit time), it is possible to extract more charge than CU. Since the extraction current is determined by the following relation $j_{SCLC} = \mathrm{CU}/t_{tr}$, the charge in the reservoir will be slowly extracted until the reservoir becomes empty due to the carrier recombination and extraction. The appearance of the characteristic extraction time t_e is seen in the current transients during the reservoir extraction. It is important to note that the reservoir extraction time t_e is larger than the carrier transit time t_{tr} and t_{cusp}, where t_{cusp} is the carrier transit time at high light intensities (e.g., for SCPC and SCLC cases). Photogenerated space charge disturbs the external applied electric field and as a result of that current transients demonstrate an initial sharp increase in current with the charge carrier transit time becoming shorter ($t_{cusp} = 0.8t_{tr}$).[13]

When further increasing the light intensity, the extracted charge will also increase until the carrier concentration becomes so high that the second order recombination starts to dominate. This is proved from the extracted charge Q_e which will saturate as a function of light intensity. Moreover, when the second order Langevin-type charge carrier recombination dominates then the extracted charge will saturate to a charge stored on the contacts CU no matter how high the pumping light intensity is (in the case of surface light absorption $\alpha d \gg 1$):[14,15]

$$Q_e/\mathrm{CU} = 1 - \exp(-Q_0/\mathrm{CU}), \tag{1}$$

where Q_e is the saturated extracted charge and Q_0 is the photogenerated charge. It is important to note that since the applied electric field is screened by both positive and negative charge carriers present inside, the electric field will be zero during carrier recombination and the diffusion controlled charge carrier recombination will dominate in the reservoir.

If the charge carriers recombine following the Langevin-type recombination, the extracted charge is approximately equal to CU, even if the amount of photogenerated charges is much larger than CU. However, it has been shown numerically that for a certain experimental conditions (e.g., volume photogeneration and low load resistance) the extracted charge can exceed CU value significantly even in case of Langevin-type carrier recombination, therefore it is important to ensure required experimental conditions when estimating the extracted charge. It is easy to show that in this case the carrier lifetime becomes equal to the transit time and even equal to the dielectric relaxation time ($\tau = t_{tr} = \tau_\sigma$).[16] The reason for the extracted charge being approximately equal to CU is that only charge approximately equal to CU can be transported at the time (SCLC condition: $j_{SCLC} = \mathrm{CU}/t_{tr}$) and while it reaches the opposite electrode the rest of charge will recombine due to the fast Langevin-type recombination in the reservoir.

The following equation has been derived to experimentally estimate the relation between the charge carrier transport and recombination in high light intensity ToF, when the extracted charge Q_e saturates as a function of light intensity:[16]

$$\frac{t_e}{t_{tr}} = \frac{\beta_L}{\beta}\frac{\mathrm{CU}}{Q_e}\frac{d_L}{d} \tag{2}$$

where β is the bimolecular recombination coefficient, d_L is the photogeneration region (e.g. surface or volume), and β_L is the Langevin recombination coefficient. All the parameters except β are known precisely from the experimental conditions.

DOI: 10.1002/pip

ToF: experimental results for MDMO-PPV/PCBM solar cells

The charge carrier mobility in MDMO-PPV/PCBM blends has been already studied before using ToF technique.[17] It was found that electron transport in PCBM is less dispersive than that of holes in MDMO-PPV in the blend, with electron mobilities in the former exceeding hole mobilities in the latter by up to two orders of magnitude. It was concluded that the photocurrent might be limited by the low hole mobility. A microscopic model for charge carrier transport and recombination has been developed to explain the recombination kinetics in MDMO:PPV/PCBM blends.[18] We present a relation between charge carrier transport and recombination measured using high light intensity ToF technique.

High light intensity ToF was used to study the carrier recombination in MDMO-PPV/PCBM blends. Our experimentally measured ToF transients for various laser intensities for MDMO-PPV/PCBM films are shown in Figure 3. The measurement parameters were: sample thickness $d = 300\,\text{nm}$, $U_0 = 2.5\,\text{V}$, $R = 4700\,\Omega$, $C = 8.85 \times 10^{-10}\,\text{F}$. Current transients are increasing with the higher light intensity with the following saturation at highest light intensities, which again demonstrates that the second order bimolecular recombination starts to dominate and limits the amount of extracted charge Q_e. However, in comparison with the RRP3HT/PCBM films (it will be shown later), the charge carrier reservoir extraction time t_e is not seen in the current transients. The extracted charge Q_e has a linear dependence in the low light intensity region and saturates at the highest light intensities because of bimolecular charge carrier recombination to the values that is close to CU_0. Moreover, the experimentally measured extraction time $t_{1/2}$ is independent of light intensity showing that the charge carriers in the reservoir are recombining within the transit time even at highest light intensities. This proves the presence of Langevin-type bimolecular charge carrier recombination in MDMO-PPV/PCBM bulk-heterojunction solar cells.

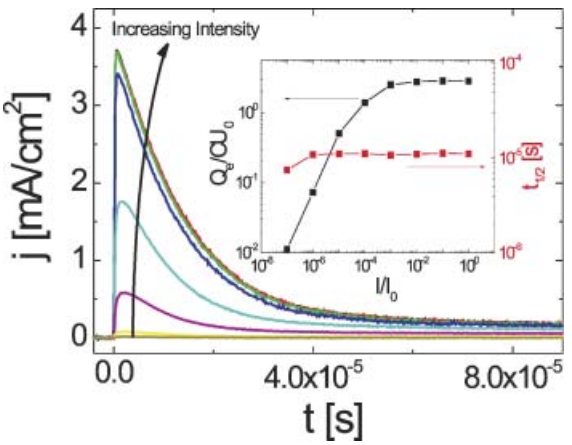

Figure 3. MDMO-PPV/PCBM bulk-heterojunction solar cells: high Intensity ToF transients, where inset shows the extracted charge and extraction half-time as a function of light intensity

It has been argued that at room temperature charge carriers can escape from the mutual Coulomb attraction and be extracted from the film using time delayed collection field technique.[19] This was explained by a screening of the Coulomb interactions or by a mechanism, in which the carriers are transported over the distances larger than Onsager radius. However, even in case of Langevin-type charge carrier recombination only CU charge can be extracted at highest possible excitation densities.

ToF: experimental results for RRP3HT/PCBM solar cells

The experimentally measured integral mode ToF ($RC \gg t_{tr}$) transients ($\tau_{RC}/t_{tr} = 10$, $\alpha' = 4$, sample thickness $d = 0.7\ \mu\text{m}$) for various laser intensities for RRP3HT/PCBM films are shown in Figure 4a. Current transients are increasing with increasing light intensity and the formation of the extraction time t_e is seen at highest light intensities. Moreover, it is seen that the transients saturate at highest light intensities. The half decay time $t_{1/2}$ is used to experimentally measure the extraction time. The current transients are integrated over time which yields the extracted charge Q_e for different light intensities shown in Figure 4b. A clear saturation of extracted charge Q_e and saturation of extraction time $t_{1/2}$ can be seen. Moreover, the extracted charge strongly exceeds the CU value ($Q_e/\text{CU} \approx 30$) and the extraction time is increasing by an order of magnitude when the intensity is increased. This demonstrates the reservoir formation and extraction at high light intensities when the bimolecular carrier recombination dominates (since Q_e saturates on light intensity) (in case when monomolecular carrier recombination dominates, the extracted charge Q_e is proportional to $\ln(L)$, where L is the light intensity.[14]). The above observations are only possible when the non-Langevin carrier bimolecular recombination is present in the films. Moreover, to prove that exactly, we calculated the bimolecular recombination coefficient $\beta = 2 \times 10^{-13}\,\text{cm}^3/\text{s}$ using Equation (2). It is impor-

DOI: 10.1002/pip

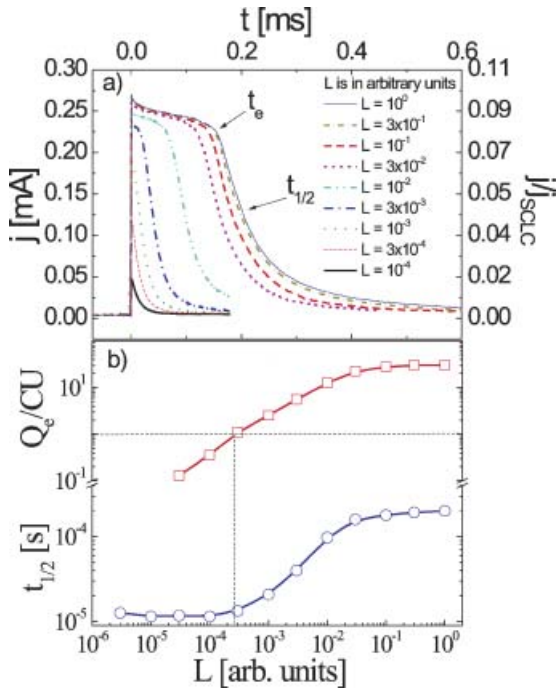

Figure 4. RRP3HT/PCBM bulk-heterojunction solar cells: experimentally measured by integral ToF transients as a function of laser light intensity in (a) and extracted charge with extraction half-time as a function of light intensity in (b). (Reprinted figure with permission from A. Pivrikas, G. Juška, A. J. Mozer, M. Scharber, K. Arlauskas, N. S. Sariciftci, H. Stubb, and R. Österbacka, *Physical Review Letters* 2005; **94**: 176806. Copyright (2005) by the American Physical Society)

tant to remember that since the electric field is screened inside the reservoir, the bimolecular recombination coefficient is estimated at zero electric field. Obtained β value is compared with the Langevin-type coefficient, which is calculated from the Langevin relation $\beta_L = e(\mu_n + \mu_p)/\epsilon\epsilon_0$,[16] using the faster carrier mobility $\mu = 4 \times 10^{-3}\,\mathrm{cm}^2/\mathrm{V\,s}$ measured from integral ToF mode. The calculated time-independent Langevin recombination coefficient [using Equation (2)] in RRP3HT/PCBM solar cells is $\beta_L = 2 \times 10^{-9}\,\mathrm{cm}^3/\mathrm{s}$. By comparing the experimentally measured bimolecular recombination coefficient with the calculated Langevin coefficient, we obtain $\beta/\beta_L = 10^{-4}$. These observations demonstrate that the bimolecular carrier recombination in thermally treated RRP3HT/PCBM bulk-heterojunction solar cells is strongly suppressed which allows for much larger charge carrier lifetimes compared to Langevin type which is typically the case for conjugated polymers and other low mobility materials. Non-Langevin carrier recombination was also observed in RRP3HT/PCBM films from the *I–V* measurements with simulations,[20] where it was explained that the recombination rate is governed by the slower charge carriers due to the confinement of both types of carriers to two different phases.

The reduced bimolecular carrier recombination in RRP3HT/PCBM solar cells is an unexpected result, since the carrier hopping distance is rather small in low mobility disordered materials and polymer/fullerene blends, implying that the photogenerated electron–hole pairs would finally recombine geminately without a possibility to escape each others Coulomb attraction.[21] The reason for the unexpected non-Langevin charge carrier recombination in RRP3HT/PCBM blends is related with the certain nanomorphology of the blends. The formation of fibrils in nanoscale and lamella-like chain packing in pure pristine RRP3HT films has been observed before.[22–27] In Figure 5 the self-alignment of RRP3HT polymer chains is shown. Two different orientations of the microcrystalline RRP3HT domains with respect to the substrate can be seen.[24]

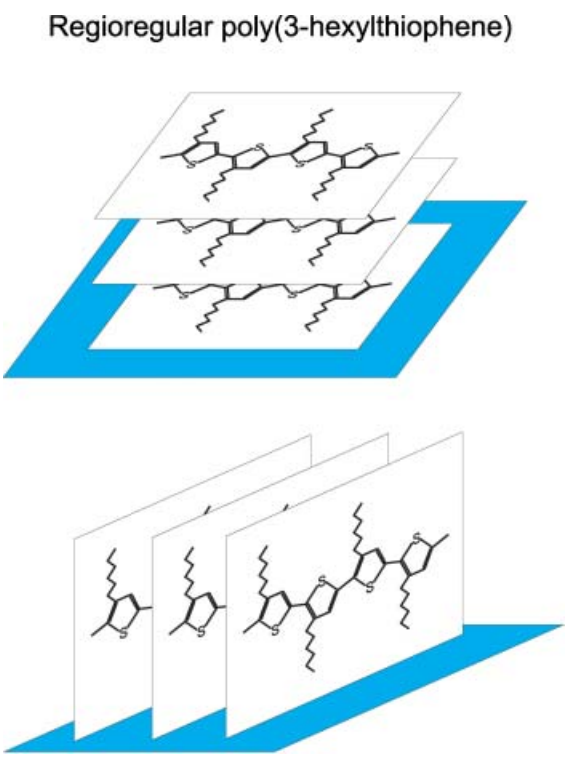

Figure 5. Two different orientations of ordered RRP3HT domains with respect to the substrate. Left picture shows horizontal stacking of RRP3HT domains, whereas right picture denotes vertical lamella stacking

DOI: 10.1002/pip

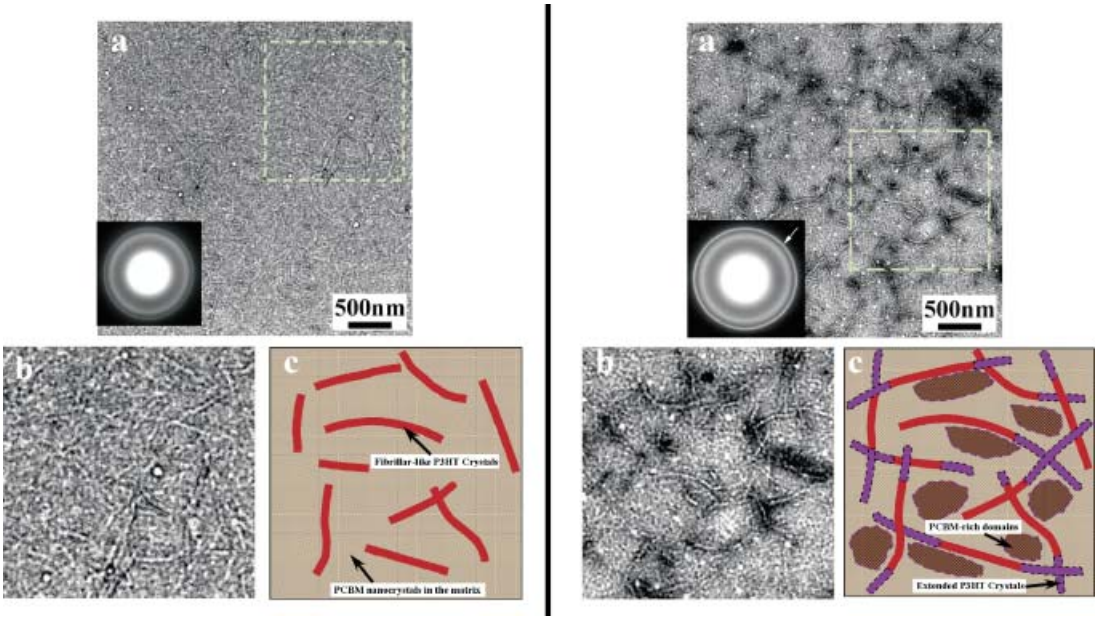

Figure 6. Left figure: BF TEM images show the overview (a) and the zoom in (b), and the corresponding schematic representation (c) of the pristine photoactive layer of a P3HT/PCBM plastic solar cell. The inset in subpart (a) is the corresponding SAED pattern. Right figure: BF TEM images show the overview (a) and the zoom in (b), and the corresponding schematic representation (c) of the thermal annealed photoactive layer. The inset in subpart (a) is the corresponding SAED pattern. Note: for right (c) Figure, the dash line bordered regions represent the extension of existing P3HT crystals in the pristine film or newly developed PCBM-rich domains during the annealing step. (Reprinted figure with permission from X. Yang, J. Loos, S. C. Veenstra, W. J. H. Verhees, M. M. Wienk, J. M. Kroon, M. A. J. Michels, and R. A. J. Janssen, *Nano Letters* 2005; **5**: 579. Copyright (2005) by the American Chemical Society)

One of the most important features of the RRP3HT/fullerene bulk-heterojunction blends is that RRP3HT retains its microcrystalline domains and chain orientation like in the pristine polymer films.[28] In Figure 6 the structural difference between the treated and untreated RRP3HT/PCBM bulk-heterojunction solar cells is seen. A polymer/fullerene phase separation process resulting from the thermal treatment or slow solvent evaporation rate during film deposition significantly changes a nanomorphology of bulk-heterojunction solar cells. A two-dimensional stacking of RRP3HT chains would result in polymer chains and microcrystalline polymer domains well aligned with the polymer/fullerene interface.

The model explaining the efficient exciton separation and reduced recombination in polymer/fullerene blends was proposed by V. I. Arkhipov. Due to the interface dipoles present at the interfaces between the donor and acceptor nanophases a Coulomb potential will form a potential barrier for carrier back-recombination.[29] At least two polymer chains parallel to the interface must be present in the blend with the interfacial dipoles created in the ground state. The reduced probability for carrier recombination in RRP3HT/PCBM blends could arise due to the screened Coulomb potential when Coulomb capture radius is approximately equal to the carrier dissipation distance, therefore, following the photoinduced charge transfer, a free mobile charge carriers can be created which then later would be transported to the electrodes either by drift or diffusion. Therefore, the interface and interaction between the RRP3HT and fullerene is crucially important for the overall properties of the blend.

Langevin-type carrier recombination in MDMO-PPV/PCBM bulk-heterojunction solar cells would imply that the carrier lifetime is much shorter compared to RRP3HT/PCBM cells at the same excitation intensities. This is also confirmed from the incident photon to current efficiency measurements, which show significantly larger efficiency values (internal quantum efficiency of the device is close to 100% at peak maximum) for RRP3HT/PCBM bulk-heterojunction solar cells.[30]

DOI: 10.1002/pip

CELIV and photo-CELIV

Time-dependent carrier mobility, lifetime and density

The CELIV technique has been introduced to study films of inorganic and organic semiconductors.[31–34] The main advantage of this technique compared to ToF is that it also allows to measure films with high bulk conductivity. Moreover, the mobility of equilibrium charge carriers and the bulk conductivity of the film can be measured under the condition that at least one blocking contact prevents carrier injection from the contact. Another unique advantage of CELIV technique is that it allows to study the relaxation of the photogenerated charge carriers in the density-of-states (DOS). Therefore, the time-dependent carrier mobility and concentration of the photogenerated charge carriers can be experimentally measured simultaneously from the current transients.[35,36]

The charge carrier transport in disordered materials is explained by carrier hopping between localized states, whereas a Gaussian DOS distribution is assumed.[37] Photogenerated charge carriers are relaxing toward lower energy states within Gaussian DOS before the thermal equilibrium is reached and carrier mobility stabilizes to a constant value. The photocurrent in non-equilibrium case is influenced by the simultaneous relaxation of both the charge carrier density and mobility, therefore it is important to understand and have experimental tools to measure both separately and simultaneously which can be done using CELIV technique.

The experimental setup and circuitry in the CELIV technique is the same as in ToF, except that a linearly increasing voltage pulse is applied. No light pulse is necessary to extract the equilibrium carriers when the system has a certain concentration of charge carriers already in the dark. When measuring undoped, low conductivity organic semiconductor films, a pumping light pulse is used to photogenerate charges prior to their extraction by the triangle voltage, implementing so called photo-CELIV technique. A schematic time diagram of the applied voltage pulse and current response is shown in Figure 7. A linearly increasing voltage pulse with the slope $A = U/t_{\text{pulse}}$ is applied to the sample to extract the equilibrium charge carriers. If the light pulse is used to photogenerate the charge carriers, the linearly increasing voltage pulse starts after some delay time t_{del}. A differentiating RC-circuit current step $j(0)$ is seen in the beginning (Figure 7). Next, the current increases due to the conductivity current (Δj) caused by the charge carriers transported in the film. The current continues to increase as the voltage increases until the charge carriers are extracted from the film and the current drops down to the capacitive step if the duration of the applied pulse is long enough and there is no carrier injection from the contacts. The characteristic extraction time t_{max} is seen in the current transients as maximum (Figure 7).

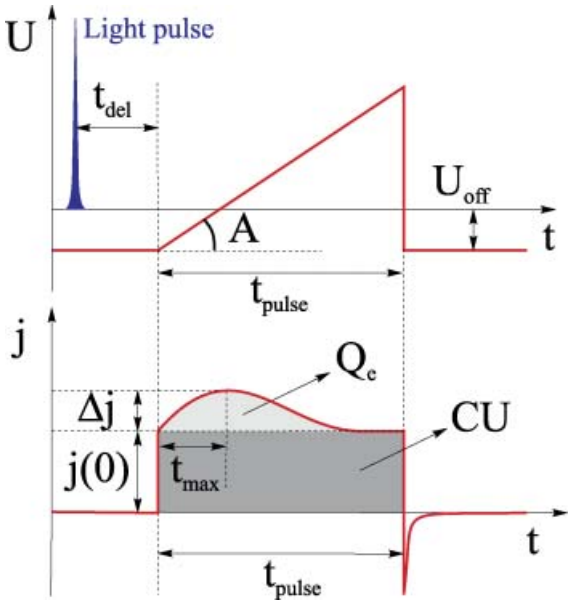

Figure 7. Applied triangle voltage pulse (top figure) and current transient response (bottom figure) in the CELIV technique. $j(0)$ represents the displacement current, whereas Δj represents the current due to transported equilibrium or photogenerated charge carriers. The extracted charge $Q_{\text{e}} = S \int_0^{t_{\text{pulse}}} \Delta j \, \text{d}t$ and $\text{CU} = S \int_0^{t_{\text{pulse}}} j(0) \, \text{d}t$, where S is the electrode area

To estimate transport parameters from CELIV we need to consider three cases depending on the conductivity of the material:[35]

1. Low conductivity case, when $\tau_\sigma \gg t_{\text{tr}}$ (or $\Delta j \ll j(0)$), where Δj is the current related to the conductivity of the film, τ_σ is the dielectric relaxation time, and $j(0)$ is the capacitive step of the current. The charge carrier mobility is directly estimated from the extraction maximum from CELIV transients:[31]

$$\mu = K \frac{d^2}{A t_{\text{max}}^2} \tag{3}$$

where $K = 2/3$ for volume and $K = 2$ for surface photogeneration, t_{max} is the time when the current reaches its highest value.

DOI: 10.1002/pip

2. High conductivity case, when $\tau_\sigma \ll t_{tr}$ (or $\Delta j \gg j(0)$). The charge carrier mobility is then estimated:[31]

$$\mu = \frac{d^2\tau_\sigma}{At_{max}^3} = \frac{d^2 j(0)}{At_{max}^2 \Delta j} \quad (4)$$

3. Moderate conductivity case, when $\tau_\sigma \approx t_{tr}$ (or $\Delta j \approx j(0)$). The charge carrier mobility is calculated from the following equation:[35]

$$\mu = K\frac{d^2}{At_{max}^2(1 + 0.36\Delta j/j(0))} \quad (5)$$

where $(1 + 0.36\Delta j/j(0))$ is the numerically calculated correction factor.

To study the density relaxation of the photogenerated charge carriers, CELIV current transients are recorded at various voltage pulse delays t_{del}. By subtracting the current transient recorded in light from the dark current transient we get the photoinduced charge carrier concentration p calculated from the extracted charge Q_e:

$$p = \frac{2Q_e}{eSd} \quad (6)$$

where S is the contact area and e is the electron charge. This simplified equation is valid for thin films and full volume photogeneration of carriers. By analyzing the experimentally measured carrier concentration as a function of t_{del} we obtain information about the carrier recombination in the time interval of the measurements.

CELIV: experimental results for RRP3HT/PCBM solar cells

CELIV transients were measured in a thick film ($d = 1.9\,\mu m$) of RRP3HT/PCBM blend. The other experimental parameters and film fabrication methods are the same as used in previous ToF measurements. Subtracted current transients (light transients minus dark) are shown in Figure 8a as a function of delay time t_{del}. In Figure 8b the carrier mobility and carrier concentration as a function of time are shown. The mobility of faster charge carriers (electrons) was measured by illuminating the sample though the ITO electrode where the negative bias was applied. The charge carrier mobility is equal to $\mu_n = 2 \times 10^{-4}\,cm^2/V\,s$ and it is independent on time in the time-window from 10^{-4} to 10^{-2} s. Since the signature of π-conjugated polymers is dispersive transport,[38–42] our observed result can be explained using Gaussian disorder formalism, where the charge carrier transport

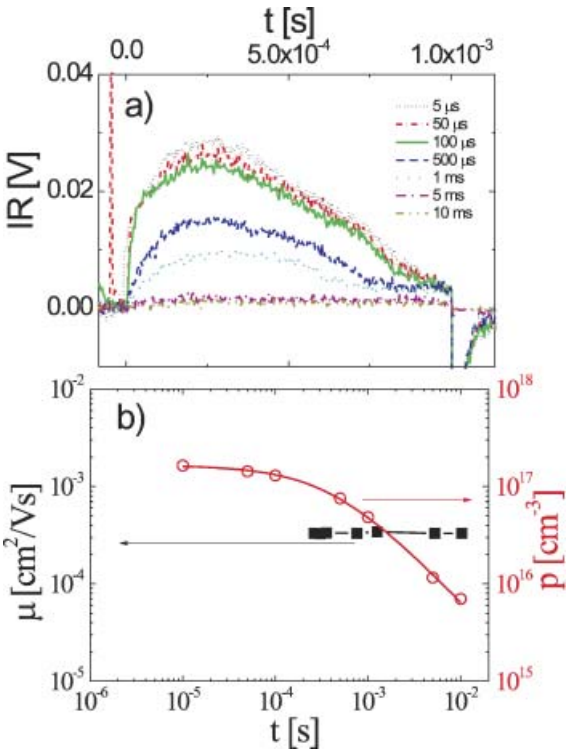

Figure 8. RRP3HT/PCBM bulk-heterojunction solar cells: current transients as a function of delay time t_{del} measured using the CELIV technique in (a) and charge carrier mobility as a function of $t_{del} + t_{max}$ (closed squares) plotted together with carrier concentration as a function of t_{del} in (b)

measured in the RRP3HT/PCBM bulk-heterojunction solar cells is present within equilibrium conditions and the carrier relaxation to the lower energy states has already happened at shorter time scales.

The measured electron mobility value is lower compared to the value measured from the ToF technique. The charge carrier mobility is strongly dependent on the disorder and nanomorphology of the studied films, since various treatment procedures and variation in sample fabrication result in significant changes in the structural morphology of the films.[43–59] The structural differences in RRP3HT/PCBM and MDMO-PPV/PCBM bulk-heterojunction solar cells were also studied using conductive atomic force microscopy, revealing that a nanoscale phase separation is present in both films.[60] CELIV method shows much stronger carrier mobility dependence on nanomorphology as it will be discussed below.

In order to study the carrier density relaxation we have measured the concentration of photogenerated charge carriers from the same CELIV transients shown

DOI: 10.1002/pip

in Figure 8a.[61] The extracted charge can also be measured by applying a simply square voltage pulse of required duration instead of the triangle to ensure that all trapped charge carriers are extracted from the film.[62] Equation (6) was used to calculate the carrier concentration which was plotted as a function of delay time t_{del}. By fitting the experimentally measured data points with the second order relaxation, the bimolecular recombination coefficient at zero electric field was obtained $\beta = 3 \times 10^{-14}\,\mathrm{cm}^3/\mathrm{s}$. Again, as in the ToF technique, we compare the experimentally measured bimolecular coefficient to the calculated Langevin coefficient and found $\beta/\beta_L = 1.7 \times 10^{-4}$. A good match between the results obtained from ToF and CELIV demonstrates that the carrier lifetime is indeed much longer (contrary to expectations from Langevin recombination) in RRP3HT/PCBM bulk-heterojunction solar cells and moreover, time-independent carrier mobility is seen from the CELIV experiment in the measured time scales. The time-independent charge carrier mobility implies that the Langevin bimolecular carrier recombination coefficient would also be time-independent in the time interval of our measurements.

CELIV: experimental results for MDMO-PPV/PCBM solar cells

The time-dependent charge carrier mobility and concentration was also studied in MDMO-PPV/PCBM bulk-heterojunction solar cells.[39] It was found that at room temperatures carrier mobility is rather weakly dependent to time t_{del}, whereas a strong dependence is seen at very low temperatures (120 K). Using the time-dependent bimolecular recombination equation, $\beta(t)$ is calculated from the experimentally measured decay of the carrier concentration and it is plotted as a function of time in Figure 9. The data reveal the power-law dependence for all temperatures. The experimentally measured time-dependent carrier mobility was compared with the time-dependence of the bimolecular recombination coefficient $\beta(t)$ obtained from the concentration decay yielding close to Langevin charge carrier recombination.

The charge carrier mobility and bimolecular lifetime were also measured in MDMO-PPV/PCBM mixtures as a function of the concentration ratio between MDMO-PPV and PCBM.[63] The product of $\mu\tau$ measured by the photo-CELIV technique at room temperature is $4 \times 10^{-10}\,\mathrm{cm}^2/\mathrm{V}$. In Figure 10 the carrier mobility is increasing with increasing PCBM concentration, whereas the carrier lifetime is

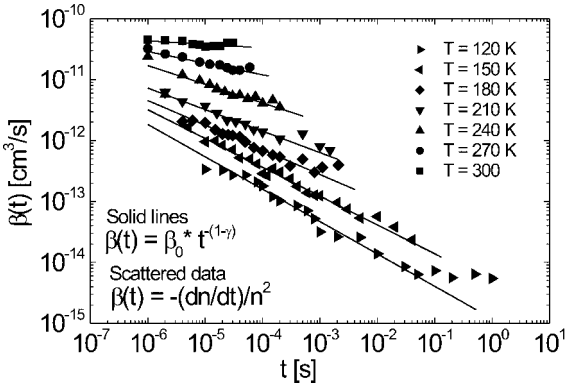

Figure 9. MDMO-PPV/PCBM bulk-heterojunction solar cells: bimolecular recombination coefficient β plotted as a function of time and fitted using time-dependent charge carrier mobility μ. (Reprinted figure with permission from A. J. Mozer, G. Dennler, N. S. Sariciftci, M. Westerling, A. Pivrikas, R. Österbacka, and G. Juška, *Physical Review B* 2005; **72**: 035217. Copyright (2005) by the American Physical Society)

decreasing. A three nanoseconds, 532 nm, 0.5 mJ/pulse, Nd-YAG laser beam was focused on 5–15 mm contact areas. When Langevin-type carrier recombination dominates, the mobility and lifetime as a function of the concentration ratio produce a constant $\mu\tau$ product, which is independent of the PCBM concentration, as shown in the inset of Figure 10. The charge carrier mobility increases by two orders of magnitude with increasing PCBM concentration, while the bimolecular

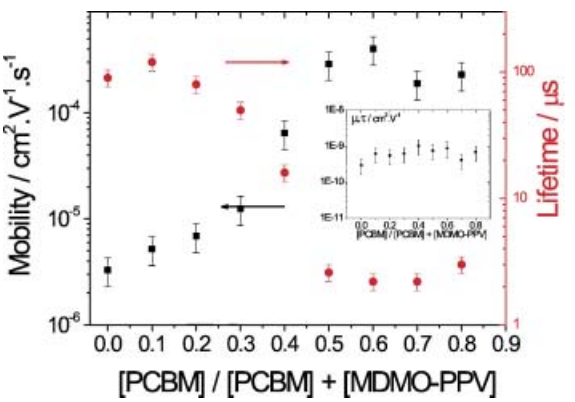

Figure 10. MDMO-PPV/PCBM bulk-heterojunction solar cells: carrier mobility μ, lifetime τ and $\mu\tau$ product versus concentration ratio of the blend. (Laser intensity used in the experiment was 0.5 mJ/pulse.) (This article was published by G. Dennler, A. J. Mozer, G. Juška, A. Pivrikas, R. Österbacka, D. A. Fuchsbauer, and N. S. Sariciftci in *Organic Electronics* 2006; **7**: 229. Copyright Elsevier (2006))

DOI: 10.1002/pip

lifetime of charge carriers strongly decreases.[48] The carrier mobility value for typical efficient blends (1:4) is rather close to what was observed before 2×10^{-4} cm^2/V s.[64]

Since the drift distance at built-in electric field is at least of the same order as the sample thickness (several hundred nanometers), a majority of the photogenerated charge carriers can be extracted from the devices under normal operational conditions with active layer thickness of the order of several hundred nanometers. Therefore, this is in agreement with the common observation that the short circuit current is not limited by second order recombination processes, but scales almost linearly with increasing incident light intensity. Langevin-type carrier recombination dominates in MDMO-PPV/PCBM blends and this bimolecular recombination does not necessarily yield to a sublinear light intensity dependence of the photocurrent.[65]

DI transients—dark current injection

Introduction to DI

We have confirmed by two independent techniques (ToF and CELIV) that the carrier lifetime is strongly increased in RRP3HT/PCBM films compared to MDMO-PPV/PCBM blends at high concentrations. What is the origin of this reduced bimolecular recombination? To elucidate this question we implemented the 'dark injection transients' to study charge carrier mobility and bimolecular recombination coefficient in RRP3HT/PCBM solar cells. The main advantage of transient techniques over stationary techniques like *I–V* measurements is that one can study the dynamics of the processes which otherwise are integrated over time. Moreover, they carry direct information about carrier transport and recombination in the films. Both electric field and temperature dependencies can be directly measured from the DI transients and since the dark injection proceeds under equilibrium conditions, the current transients are less influenced by carrier relaxation in the DOS as it is the case with photogenerated current transients. Bipolar charge carrier transport has already been studied before, showing that the nanomorphology and the structure of the percolating networks are extremely important for the charge carrier transport.[66] DI method has been used before to study charge carrier injection in silicon p-i-n diodes,[67,68] and germanium.[69] DI transients were also studied in silicon,[70] in semiconductors with[71] and without traps.[72] DI into the semiconductors and intrinsic conductors[73] was clarified in the presence of first and second order carrier recombination, including carrier trapping and diffusion.[13,74] However, DI into insulators has not been studied widely and an exact analytical solution to describe the DI current transients is not available.

The experimental setup for DI transient measurements is the same as in ToF technique, except that no light is required for DI since the charge carriers are injected from the opposite electrodes. Square voltage pulse in forward bias with the amplitude U and duration t_{pulse} is applied to inject electrons and holes into the film and the current response is recorded in the oscilloscope. A schematic figure of the applied voltage and current response are shown in Figure 11a and b. The dark

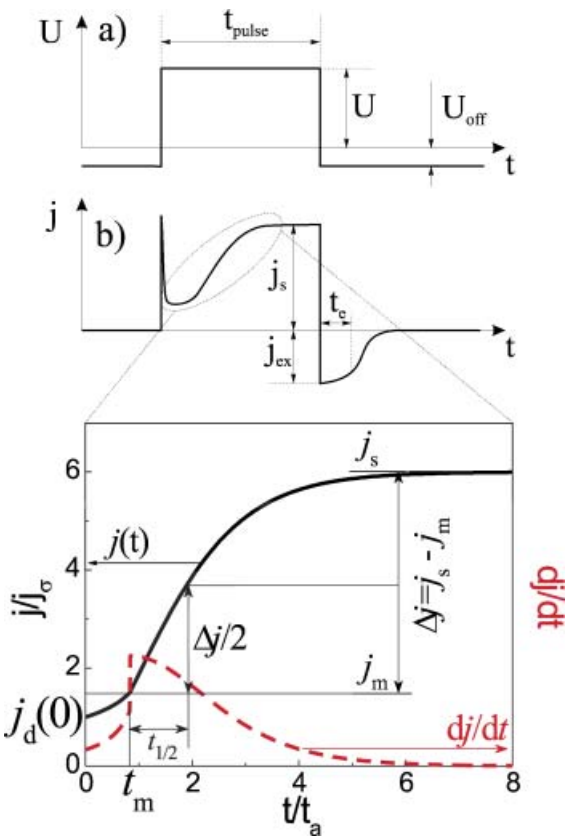

Figure 11. DI transient technique: applied voltage pulse (a) and current transient response recorded in the oscilloscope (b). An ideal DI current transient with characteristic current increase after *RC* spike is shown. At the end of applied voltage pulse plasma extraction time t_e is also seen in the current transient. In the magnified picture: the solid line shows the ideal DI current transient, whereas the dashed line shows the time-derivative of the DI transient

DOI: 10.1002/pip

current transient response in Figure 11b shows an *RC* decay immediately after the application of the external voltage pulse. Later, the current starts to increase until it reaches saturated value j_s due to carrier recombination. The current increase is related to the plasma formation in the film, when the amount of charge carriers is much larger compared to what is stored on the electrodes (CU/e). In general, the ratio of injected charge to injected plasma Q/end will depend on the ratio of the sum of carrier mobilities $t_{tr}^{n} + t_{tr}^{p}$ to carrier lifetime τ: $Q/\text{end} = (t_{tr}^{n} + t_{tr}^{p})/\tau$.[13] Depending on the relation between the film conductivity ($\sigma = \epsilon\epsilon_0/\tau_\sigma$) and charge carrier transit time, two cases of DI are possible:[13]

1. $\tau_\sigma \ll t_{tr}$—DI into high conductivity semiconductor.

   The saturated DI current j_s into the high conductivity semiconductor, limited by bimolecular recombination can be written as:[13]

$$j_s = \frac{8e}{9}\sqrt{\frac{(\mu_n + \mu_p)\mu_n\mu_p(n_0 - p_0)}{\beta}}\frac{U^{3/2}}{d^2} = \frac{8}{9}\frac{U}{d}\epsilon\epsilon_0\sqrt{\frac{\beta_L}{\beta}\frac{1}{\tau_\sigma t_a}} \quad (7)$$

   where n_0 (p_0) is the concentration of electrons (holes) and t_a is the ambipolar charge carrier transit time.

   In this case the DI current transients can be expressed as:[13]

$$j(t) = \begin{cases} \sigma E\left(1 - \frac{2}{3}\frac{t}{t_a}\right)^{-\frac{1}{2}}, & t < \frac{5}{6}t_a \\ \frac{3}{2}\sigma E + \left(j_s - \frac{3}{2}\sigma E\right)\tanh\left(\beta\Delta n_s\left(t - \frac{5}{6}t_a\right)\right), & t > \frac{5}{6}t_a \end{cases} \quad (8)$$

   where σ is the conductivity of the film and Δn_s is the saturated concentration of injected charge carriers.

   The ambipolar charge carrier mobility μ_a can be experimentally estimated from the ambipolar carrier transit time t_a. However, t_a is not clearly seen in the DI transients, but by taking the derivative of the DI current (Figure 11) we can experimentally measure the inflection point t_m, which will be related with the ambipolar carrier transit time t_a as:[13]

$$t_a = \frac{d^2}{\mu_a U} = \frac{5d^2}{6t_m U} \quad (9)$$

   where $t_m = 5/6t_a$ is the maximum position of the current derivative (see Figure 11). The ambipolar charge carrier mobility μ_a can be also written as:[13]

$$\mu_a = \frac{n_0 - p_0}{\frac{n}{\mu_p} + \frac{p}{\mu_n}} = \frac{e}{\sigma}\mu_n\mu_p(n_0 - p_0) \quad (10)$$

   which demonstrates that in general it is determined by the mobility of minority carriers.

   When the DI current at zero time $j_d(0)$ is much smaller than the saturated current value ($j_d(0) \ll j_s$, see Figure 11) another equation is used to calculate β/β_L:[75]

$$\frac{\beta}{\beta_L} = 0.45\frac{\tau_\sigma t_m}{t_{1/2}^2} \quad (11)$$

2. $\tau_\sigma \gg t_{tr}$—DI into low conductivity semiconductor (insulator).

   The saturated current j_s, in case of injection into a low conductivity semiconductor limited by bimolecular recombination, is derived elsewhere:[13]

$$j_s = \sqrt{\frac{9\pi}{4}}\sqrt{\frac{e\mu_p\mu_n(\mu_p + \mu_n)\epsilon\epsilon_0}{\beta}}\frac{U^2}{d^3} = \epsilon\epsilon_0\sqrt{\frac{9\pi}{4}}\sqrt{\frac{\beta_L}{\beta}\mu_n\mu_p}\frac{U^2}{d^3} \quad (12)$$

   It is important to note that the power-law dependence with a slope of 2 might look like the typical SCLC current (unipolar injection in case $\tau_\sigma \gg t_{tr}$), therefore, the *I–V* dependence alone can be misleading due to integral nature of this technique.

   Since there is no simple analytical solution to describe the DI current transients into an insulator limited by bimolecular recombination, however, the DI current transients can be generalized to:[76]

$$j(t) \propto \tanh(\beta\Delta n_s t) \quad (13)$$

   where Δn_s is the density of the saturated plasma as a function of time t. The mobility of both faster and slower charge carriers can be directly estimated from the DI transients and by measuring the maximum points of the time-derivative of the current transient.[77]

The DI transients allow us to directly estimate the bimolecular recombination coefficient, when there is a reduced (non-Langevin) bimolecular recombination present. An analytical solution to calculate the ratio of the bimolecular recombination coefficient with

DOI: 10.1002/pip

Langevin coefficient (β/β_L) is derived:[75]

$$\frac{\beta}{\beta_L} = \frac{\ln 3}{2}\frac{\epsilon\epsilon_0 U}{d}\frac{1}{t_{1/2}\Delta j} \quad (14)$$

where Δj and $t_{1/2}$ are shown in Figure 11.

By using both Equations (11) and (14) it is possible to measure the electric field and temperature dependence of the bimolecular recombination coefficients directly from the DI transients without using data fitting and without setting up transport-recombination models. Therefore, once it is possible to apply this technique, it is very powerful tool to study the charge carrier transport and recombination in organic semiconductors.

DI results in RRP3HT/PCBM solar cells

As we have already seen the DI transients and the saturated current value j_s will be different depending where the DI into the high or low conductivity semiconductor is present. We experimentally have measured the DI current transients in both cases for RRP3HT/PCBM bulk-heterojunction solar cells. The film conductivity was measured using dark CELIV technique. The films with high or low conductivity were obtained by choosing various film preparation procedures.[50]

The *I–V* dependence was measured for two types of efficient RRP3HT/PCBM bulk-heterojunction solar cells: both high and low conductivity cells (see Figure 12). The current density at the voltages above the built-in field is proportional to the voltage square in case of DI into insulator [Equation (7)] and proportional to voltage power three half in case of injection into high conductivity semiconductor [Equation (12)]. However, since the stationary current is influenced by many factors including contacts, various trapping effects, and other phenomena, the dark current dependence has to be justified. The following sections deal with the dark current transients which demonstrate that the observed effects are truly intrinsic property of the material with respect to experimental conditions.

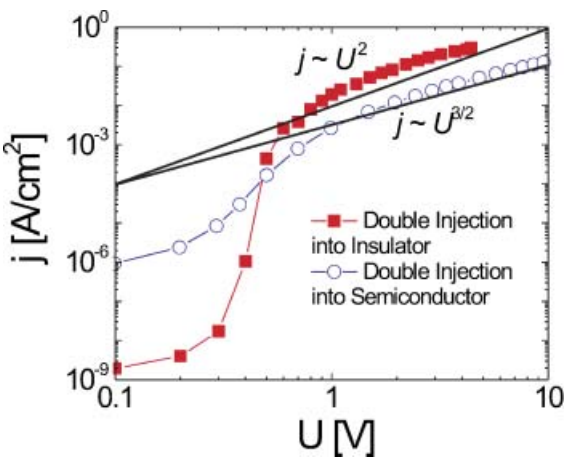

Figure 12. RRP3HT/PCBM bulk-heterojunction solar cells: *I–V* dependence in high and low conductivity films

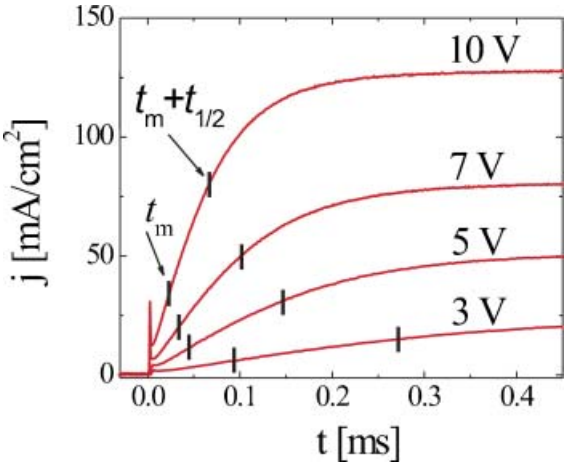

Figure 13. RRP3HT/PCBM bulk-heterojunction solar cells: DI current transients for different applied voltages. The dashes show maximum points t_m of the current derivative and $t_m + t_{1/2}$ time used to directly calculate carrier mobility and bimolecular recombination coefficient β for different applied voltages

Experimentally measured dark current transients as a function of applied voltage in RRP3HT/PCBM mixtures are shown in Figure 13. These DI current transients were measured in bulk-heterojunction solar cells, where the condition $\tau_\sigma \ll t_{tr}$ is valid, meaning that the DI into high conductivity semiconductor mode is ensured. The current resembles typical DI current transients as it is shown in Figure 11. The saturated dark current j_s reaches higher values for higher applied voltages U. From the maximum inflection points t_m the ambipolar carrier mobility and from $t_{1/2}$ bimolecular recombination coefficient are estimated.

In order to estimate the dependence of carrier mobility and bimolecular recombination coefficient on the electric field and temperature, the ratio β/μ is calculated. In case of Langevin-type carrier recombination the ratio is expected to be constant, as it was already demonstrated from CELIV measurements in MDMO-PPV/PCBM solar cells. The ratio of the bimolecular recombination coefficient to the carrier mobility as a function of electric field is plotted in Figure 14 for three different temperatures (197, 251, and 290 K). The dependence of β/μ ratio is

DOI: 10.1002/pip

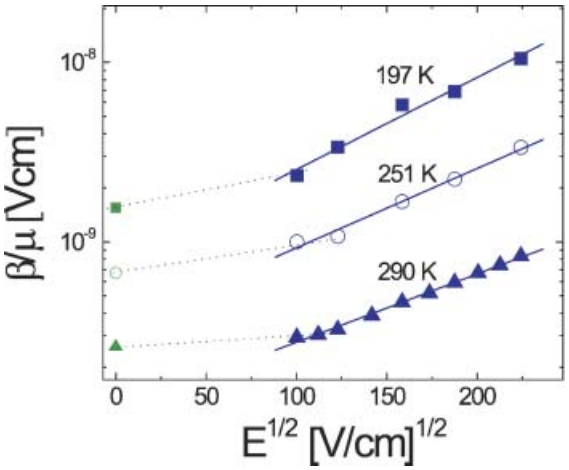

Figure 14. RRP3HT/PCBM bulk-heterojunction solar cells: ratio of the bimolecular recombination coefficient β with charge carrier mobility μ as a function of electric field

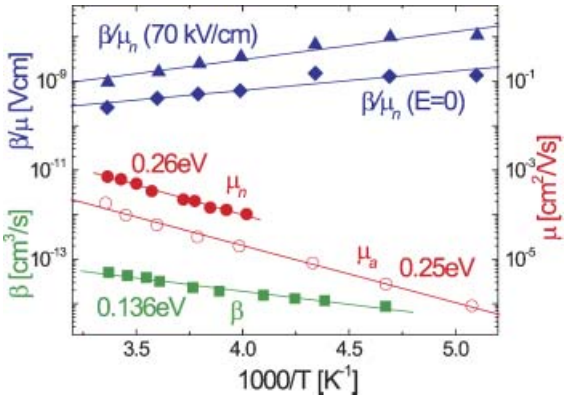

Figure 15. RRP3HT/PCBM bulk-heterojunction solar cells: electron mobility μ_n, ambipolar carrier mobility μ_a, bimolecular recombination coefficient β, and the ratio of both as a function of temperature

extended to zero electric field (data point connected with dotted line) using the data obtained from high laser intensity ToF technique. All measured data points for different temperatures show similar dependence on electric field. The electric field dependence of bimolecular recombination coefficient in low mobility media has been modeled before showing that β should have a slight decrease at high electric fields.[78] The non-constant dependence of β/μ ratio demonstrates that the electric field dependence of reduced carrier recombination coefficient is not completely governed by the carrier mobility as it is in the case of Langevin recombination.

The bimolecular recombination coefficient, carrier mobility, and the ratio of them plotted as a function of temperature is shown in Figure 15. The ambipolar charge carrier mobility μ_a and β were estimated directly from the DI current transients recorded at various temperatures. In the same figure we show the faster carrier (electron) mobility μ_n as a function of temperature measured with CELIV method for a fixed delay time t_{del}. The activation energy of the faster charge carrier mobility is $\Delta_n = 0.26\,eV$ and for ambipolar carrier mobility $\Delta_a = 0.25\,eV$, whereas for the bimolecular recombination coefficient $\Delta_\beta = 0.136\,eV$. The temperature dependence of β is weaker compared to carrier mobility which is an opposite result compared to Langevin-type carrier recombination.

In RRP3HT/PCBM bulk-heteronjunction solar cells using *I–V* measurements the hole mobility has been measured to be in the range 10^{-6}–10^{-4}.[79,80] Using field effect measurements it was found that in efficient 1:2 RRP3HT/PCBM ratio electron and hole mobility is balanced and approximately equal to $10^{-3}\,cm^2/V\,s$.[81]

Plasma extraction technique

Introduction to plasma extraction

The plasma extraction technique described below is complementary to the DI current transient technique since it allows measuring samples with high capacitance or high contact resistance, which is impossible with previous technique due to larger *RC* time constant and low actual applied voltages on the film.[76]

An experimental setup is the same as in DI current transient measurements. During application of the square voltage pulse in forward bias (see Figure 16) the charge carriers are injected into the film. Due to the long charge carrier lifetime (carrier lifetime is longer than transit time due to reduced bimolecular recombination), plasma with the large amount of charge carriers is formed ($e(N + P) \gg$ CU, where $N(P)$ is the number of electrons (holes)) during the injection. The idea with plasma extraction is that when the carrier injection in forward bias stops (end of the t_{pulse}), the negative offset voltage in reverse bias U_{off} is restored to extract the formed plasma from the film. A characteristic extraction current j_{ex} and extraction time t_e are seen in the extraction current transients in Figure 16.

To better understand the plasma formation and extraction, the following transients demonstrating plasma extraction are shown in Figure 17. The reservoir extraction can be controlled by changing the applied

DOI: 10.1002/pip

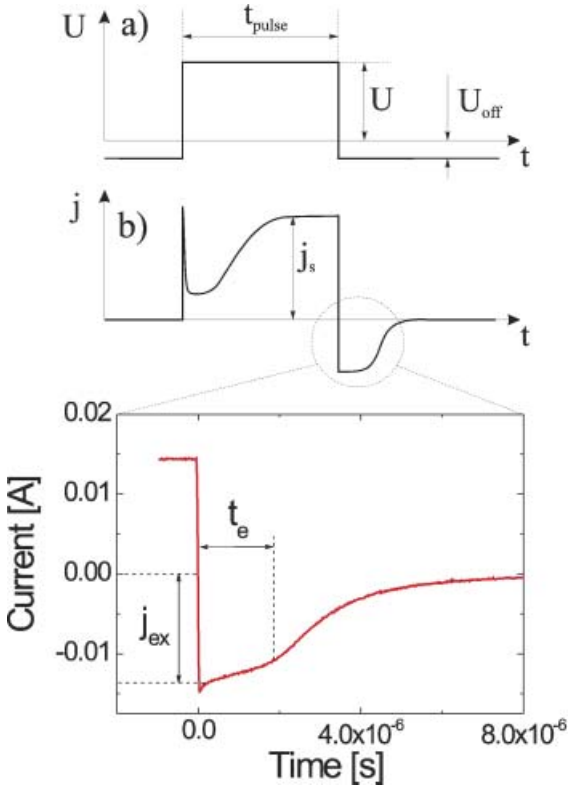

Figure 16. Plasma extraction technique: applied voltage pulse (a) and current transient response recorded in the oscilloscope (b). An experimental current transient with characteristic reservoir extraction t_e is shown in the magnified picture

voltage in forward bias U, the offset voltage U_{off}, and the pulse duration. With higher forward bias voltage the saturated current increases and the amount of charge carriers forming plasma also increases (can then be seen from increasing extraction transients). When the offset voltage is increased, the amount of extracted charge stays roughly the same (some carriers are lost due to recombination at low offset voltages), but the extraction time becomes shorter and extraction transients become steeper. When the pulse duration in forward bias is changed, the amount of injected charge varies (from $\ll$ CU to $\gg$ CU), where the later corresponds to plasma formed in the film.

The essence of this technique is that the carrier mobility μ and bimolecular recombination coefficient β can be estimated from the saturated injected charge Q_s. Since it is experimentally difficult to estimate Q_s during injection, we measure the extracted charge Q_e choosing experimental conditions such, that there are no carrier losses due to recombination during extraction.

Simple analytical solution to calculate the bimolecular recombination coefficient from the saturated injected charge Q_s is derived:[76]

$$\beta = \frac{\ln 3}{2}\frac{edS}{t_{Q/2}Q_s} \tag{15}$$

where $t_{Q/2}$ is the time when the injected charge is equal to half of its maximum value. However, experimentally we measure the Q_s from the extracted charge Q_{ex}, knowing that we extract all charge without significant carrier recombination.

The sum of carrier mobilities is estimated from the injected charge by measuring the Q_s and the saturated current j_s:

$$t_{tr} = \frac{d^2}{(\mu_n + \mu_p)U} = \frac{Q_s}{j_s S} \tag{16}$$

The sum of the carrier mobilities can also be estimated from the time when the pulse duration is such that extracted (injected) charge is equal to CU:[13]

$$Q_s(t_p) = \text{CU}, \text{ when } t_p = t_{tr} \tag{17}$$

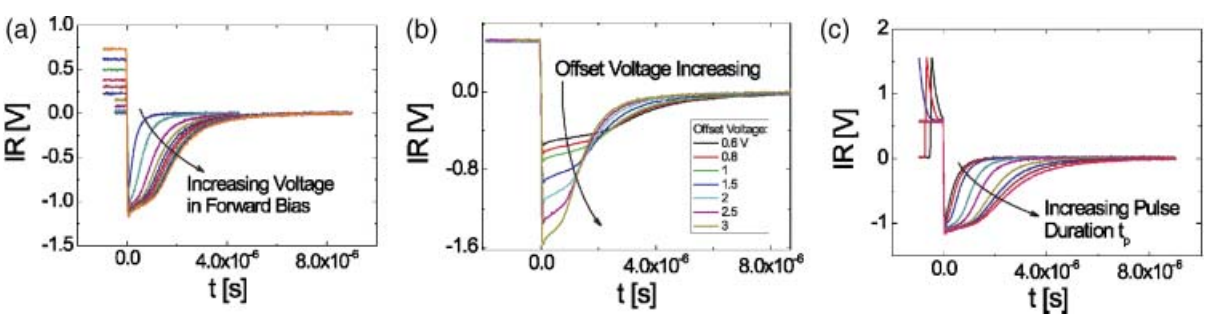

Figure 17. RRP3HT/PCBM bulk-heterojunction solar cells: plasma extraction current transients shown as a function of applied voltage in forward bias U (a), as a function of offset voltage U_{off} (b), and as a function of pulse duration t_p (c)

DOI: 10.1002/pip

The mobility of slower charge carriers can be directly estimated from the kink in DI transients. The time $t_p = t_{tr}$ is taken from the derivative of the extracted charge as a function of t_p.[77]

Plasma extraction results for RRP3HT/PCBM solar cells

An experimentally measured extracted charge in RRP3HT/PCBM blend is shown in Figure 18. The low conductivity samples were measured ensuring the condition $\tau_\sigma \gg t_{tr}$ (DI into insulator). However, it is not necessary to fulfill this condition in order to be able to apply plasma extraction technique. As can be seen from Figure 18, the extracted charge at highest pulse durations is much larger than CU ($Q_{ex} \gg$ CU) which confirms the plasma formation.

Using Equations (16) and (17) the carrier transit time t_{tr} was estimated and the sum of both charge carrier mobilities ($\mu_n + \mu_p$) was found and from both equations it is approximately equal to $0.01\,cm^2/V\,s$. The mobility of slower carriers (holes) is also estimated from Figure 18 $\mu_h = 2 \times 10^{-3}\,cm^2/V\,s$. The obtained charge carrier mobility values are rather close to an electron mobility in pure C_{60} films,[82] however, it is also strongly dependent on the nanomorphology of the films and disorder.[83]

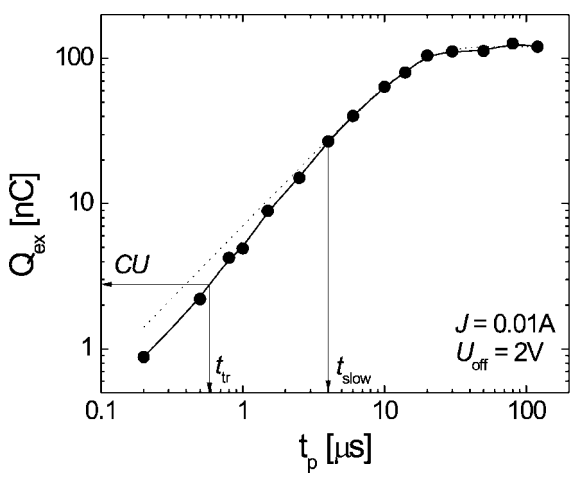

Figure 18. RRP3HT/PCBM bulk-heterojunction solar cells: experimentally measured extracted charge as a function of pulse duration t_p. Dotted line shows the functional dependence of extracted charge. Both the sum of electron and hole mobilities (from t_{tr}) and the mobility of slower charge carriers (from t_{slow}) can be directly estimated from the figure. (Reprinted figure with permission from G. Juška, K. Genevičius, G. Sliaužys, A. Pivrikas, M. Scharber and R. Österbacka, *Journal of Applied Physics*, in print, 2007. Copyright (2007) by the American Institute of Physics)

The bimolecular recombination coefficient β was calculated using Equation (15) from half of the extracted charge $Q_{ex}/2$ and half-extraction time $t_{Q/2}$. The obtained value bimolecular recombination coefficient in RRP3HT/PCBM bulk-heterojunction solar cells is $\beta = 2.2 \times 10^{-12}\,cm^3/s$ at an electric field $E \approx 10^4\,V/cm$.

CONCLUSIONS

It was shown by ToF, CELIV, DI transient, Plasma extraction and *I–V* techniques the charge carrier mobility, bimolecular recombination coefficient, and bimolecular carrier lifetime can be measured simultaneously and comparatively. In two polymer/fullerene mixtures: RRP3HT/PCBM and in the blend of MDMO-PPV mixed with PCBM (MDMO-PPV/PCBM) we have studied the transport and recombination. The mobility of faster carriers was found to be larger in thermally treated highly efficient RRP3HT/PCBM films and the recombination is strongly suppressed as compared to Langevin recombination (*ca* 10^{-4} times). It is shown that the carrier mobility is strongly dependent on the film morphology and disorder. Therefore, as it is demonstrated in the number of publication, the carrier mobility can change orders of magnitude depending on the film preparation techniques, solvents used for film deposition, time, and temperature of the thermal treatment, etc. A unique possibility to experimentally measure the time-dependent carrier mobility is shown using CELIV technique. It was found that mobility is independent on time in RRP3HT/PCBM blends in the time scales of the experiment (approx. hundreds of microseconds to tens of milliseconds), whereas in MDMO-PPV blends carrier mobility has a stronger time-dependence at room temperatures. The reduced carrier bimolecular recombination compared to Langevin type is observed in RRP3HT/PCBM blends, whereas in MDMO-PPV/PCBM blends there is Langevin-type recombination. The experimentally measured bimolecular recombination coefficient ratio with Langevin-type coefficient for efficient RRP3HT/PCBM blends is $\beta/\beta_L = 10^{-4}$ and for MDMO-PPV/PCBM blends $\beta/\beta_L \approx 1$. As a result of non-Langevin carrier recombination much longer charge carrier lifetimes can be achieved in RRP3HT/PCBM films under the operational conditions at high carrier concentrations.

DOI: 10.1002/pip

Explaining the reduced carrier recombination requires structural order in the presence of interface dipoles which would create a potential barrier for carrier recombination. The specific nanomorphology of RRP3HT/PCBM blends could result in screened Coulomb potential between the photoexcitations at the interface and facilitate the splitting of photoexcitations into free charge carriers with the following reduced recombination probability.

Acknowledgments

We thank K. Arlauskas, K. Genevičius, M. Scharber, G. Dennler, A. J. Mozer for valuable discussions. Financial support from the Academy of Finland through Contract No. 107684, the Lithuanian State Science and Studies Foundation through Contract No. C-19/2007 is acknowledged. Partial financial support of Austrian Foundation for Advancement of Science (FWF) is acknowledged.

REFERENCES

1. Chamberlain GA. Organic solar cells: a review. *Solar Cells* 1983; **8**: 47–83.
2. Wöhrle D, Meissner D. Organic solar cells. *Advanced Materials* 1991; **3**: 129–138.
3. Brabec CJ, Sariciftci NS, Hummelen JC. Plastic solar cells. *Advanced Functional Materials* 2001; **11**: 15–26.
4. Nelson J. Organic photovoltaic films. *Current Opinion in Solid State & Materials Science* 2002; **6**: 87–95.
5. Nunzi J-M. Organic photovoltaic materials and devices. *Comptes Rendus Physique* 2002; **3**: 523–542.
6. Brabec CJ, Dyakonov V, Parisi J, Sariciftci NS (eds). *Organic Photovoltaics: Concepts and Realization*, vol. 60. Springer: Berlin, Germany, 2003.
7. Peumans P, Yakimov A, Forrest SR. Small molecular weight organic thin-film photodetectors and solar cells. *Journal of Applied Physics* 2003; **93**: 3693–3723.
8. Janssen RAJ, Hummelen JC, Sariciftci NS. Polymer-fullerene bulk heterojunction solar cells. *MRS Bulletin* 2005; **30**: 33–36.
9. Forrest SR. The limits to organic photovoltaic cell efficiency. *MRS Bulletin* 2005; **30**: 28–32.
10. Pai DM, Enck RC. Onsager mechanism of photogeneration in amorphous selenium. *Physical Review B* 1975; **11**: 5163–5174.
11. Österbacka R, Juška G, Arlauskas K, Pal AJ, Källman K-M, Stubb H. Electric field redistribution and electroluminescence response time in polymeric light-emitting diodes. *Journal of Applied Physics* 1998; **84**: 3359–3363.
12. Pivrikas A, Juška G, Mozer AJ, Scharber M, Arlauskas K, Sariciftci NS, Stubb H, Österbacka R. Bimolecular recombination coefficient as a sensitive testing parameter for low-mobility solar-cell materials. *Physical Review Letters* 2005; **94**: 176806-1–176806-4.
13. Lampert MA, Mark P. *Current Injection in Solids*. Academic Press: New York and London, 1970.
14. Juška G, Viliūnas M, Arlauskas K, Kočka J. Space-charge-limited photocurrent transients: the influence of bimolecular recombination. *Physical Review B* 1995; **51**: 16668–16676.
15. Kočka J, Klíma O, Juška G, Hoheisel O, Plättner R. SCLC transients in a-Si:H : new features and possibilities. *Journal of Non-Crystalline Solids* 1991; **137**: 427–430.
16. Pivrikas A, Juška G, Österbacka R, Westerling M, Viliūnas M, Arlauskas K, Stubb H. Langevin recombination and space-charge-perturbed current transients in regiorandom poly(3-hexylthiophene). *Physical Review B* 2005; **71**: 125205-1–125205-5.
17. Choulis SA, Nelson J, Kim Y, Poplavskyy D, Kreouzis T, Durrant JR, Bradley DDC. Investigation of transport properties in polymer/fullerene blends using time-of-flight photocurrent measurements. *Applied Physics Letters* 2003; **83**: 3812–3814.
18. Nelson J, Choulis SA, Durrant JR. Charge recombination in polymer/fullerene photovoltaic devices. *Thin Solid Films* 2004; **451**: 508–514.
19. Offermans T, Meskers SCJ, Janssen RAJ. Time delayed collection field experiments on polymer: fullerene bulk-heterojunction solar cells. *Journal of Applied Physics* 2006; **100**: 074509-1–074509-7.
20. Koster LJA, Mihailetchi VD, Blom PWM. Bimolecular recombination in polymer/fullerene bulk heterojunction solar cells. *Applied Physics Letters* 2006; **88**: 052104-1–052104-3.
21. Arkhipov VI, Emelianova EV, Barth S, Bässler H. Ultrafast on-chain dissociation of hot excitons in conjugated polymers. *Physical Review B* 2000; **61**: 8207–8214.
22. Prosa TJ, Winokur MJ, McCullough RD. Evidence of a novel side chain structure in regioregular poly(3-alkylthiophenes). *Macromolecules* 1996; **29**: 3654–3656.
23. Bao Z, Dodabalapur A, Lovinger AJ. Soluble and processable regioregular poly(3-hexylthiophene) for thin film field-effect transistor applications with high mobility. *Applied Physics Letters* 1996; **69**: 4108–4110.
24. Sirringhaus H, Brown PJ, Friend RH, Nielsen MM, Bechgaard K, Langeveld-Voss BMW, Spiering AJH, Janssen RAJ, Meijer EW, Herwig P, de Leeuw DM. Two-dimensional charge transport in self-organized, high-mobility conjugated polymers. *Nature* 1999; **401**: 685–687.
25. Österbacka R, An CP, Jiang XM, Vardeny ZV. Two-dimensional electronic excitations in self-assembled

DOI: 10.1002/pip

Conjugated Polymer Nanocrystals. *Science* 2000; **287**: 839–841.
26. Savenije TJ, Kroeze JE, Yang X, Loos J. The formation of crystalline P3HT fibrils upon annealing of a PCBM:P3HT bulk heterojunction. *Thin Solid Films* 2006; **511**: 2–6.
27. Kline RJ, McGehee MD, Toney MF. Highly oriented crystals at the buried interface in polythiophene thin-film transistors. *Nature Materials* 2006; **5**: 222–228.
28. Kim Y, Cook S, Tuladhar SM, Choulis SA, Nelson J, Durrant JR, Bradley DDC, Giles M, McCulloch I, C.-S. Ha, Ree M. A strong regioregularity effect in self-organizing conjugated polymer films and high-efficiency polythiophene: fullerene solar cells. *Nature Materials* 2006; **5**: 197–203.
29. Arkhipov VI, Heremans P, Bässler H. Why is exciton dissociation so efficient at the interface between a conjugated polymer and an electron acceptor? *Applied Physics Letters* 2003; **82**: 4605–4607.
30. Schilinsky P, Waldauf C, Brabec CJ. Recombination and loss analysis in polythiophene based bulk heterojunction photodetectors. *Applied Physics Letters* 2002; **81**: 3885–3887.
31. Juška G, Arlauskas K, Viliūnas M, Kočka J. Extraction current transients: new method of study of charge transport in microcrystalline silicon. *Physical Review Letters* 2000; **84**: 4946–4949.
32. G. Juška, Viliūnas M, Arlauskas K, Nekrašas N, Wyrsch N, Feitknecht L. Hole drift mobility in μc-Si:H. *Journal of Applied Physics* 2001; **89**: 4971–4974.
33. Juška G, Genevičius K, Viliūnas M, Arlauskas K, Stuchlíková H, Fejfar A, Kočka J. New method of drift mobility evaluation in muc-Si:H, basic idea and comparison with time-of-flight. *Journal of Non-Crystalline Solids* 2000; **266**: 331–335.
34. Juška G, Arlauskas K, Österbacka R, Stubb H. Time-of-flight measurements in thin films of regioregular poly(3-hexyl thiophene). *Synthetic Metals* 2000; **109**: 173–176.
35. Juška G, Arlauskas K, Viliūnas M, K. Genevičius, Österbacka R, Stubb H. Charge transport in pi-conjugated polymers from extraction current transients. *Physical Review B* 2000; **62**: R16235–R16238.
36. Genevičius K, Österbacka R, Juška G, Arlauskas K, Stubb H. Charge transport in pi-conjugated polymers from extraction current transients. *Thin Solid Films* 2002; **403**: 415–418.
37. Bässler H. Charge transport in disordered organic photoconductors. A Monte Carlo Simulation Study. *Physica Status Solidi (b)* 1993; **175**: 15–56.
38. Pivrikas A, Österbacka R, Juška G, Arlauskas K, Stubb H. Time-dependent Langevin-type bimolecular charge carrier recombination in regiorandom poly(3-hexylthiophene). *Synthetic Metals* 2005; **155**: 242–245.
39. Mozer AJ, Dennler G, Sariciftci NS, Westerling M, Pivrikas A, Österbacka R, Juška G. Time-dependent mobility and recombination of the photoinduced charge carriers in conjugated polymer/fullerene bulk heterojunction solar cells. *Physical Review B* 2005; **72**: 035217-1–035217-10.
40. Österbacka R, Pivrikas A, Juška G, Genevičius K, Arlauskas K, Stubb H. Mobility and density relaxation of photogenerated charge carriers in organic materials. *Current Applied Physics* 2004; **4**: 534–538.
41. Pivrikas A, Österbacka R, Juška G, Arlauskas K, Stubb H. Time-dependent Langevin-type bimolecular charge carrier recombination in regiorandom poly(3-hexylthiophene). *Synthetic Metals* 2005; **155**: 242–245.
42. Mozer A, Sariciftci NS, Pivrikas A, Österbacka R, Juška G, Bässler H. Charge carrier mobility in regioregular poly(3-hexylthiophene) probed by transient conductivity techniques: a comparative study. *Physical Review B* 2005; **71**: 035214-1–035214-9.
43. Peumans P, Uchida S, Forrest SR. Efficient bulk heterojunction photovoltaic cells using small-molecular-weight organic thin films. *Nature* 2003; **425**: 158–162.
44. Hoppe H, Sariciftci NS. Organic solar cells: an overview. *Journal of Materials Research* 2004; **19**: 1924–1945.
45. Chirvase D, Parisi J, Hummelen JC, Dyakonov V. Influence of nanomorphology on the photovoltaic action of polymer-fullerene composites. *Nanotechnology* 2004; **15**: 1317–1323.
46. Mihailetchi VD, Xie HX, de Boer B, Koster LJA, Blom PWM. Charge transport and photocurrent generation in poly(3-hexylthiophene): methanofullerene bulk-heterojunction solar cells. *Advanced Functional Materials* 2006; **16**: 699–708.
47. Kim Y, Choulis SA, Nelson J, Bradley DDC, Cook S, Durrant JR. Composition and annealing effects in polythiophene/fullerene solar cells. *Journal of Materials Science* 2005; **40**: 1371–1376.
48. Mihailetchi VD, Koster LJA, Blom PWM, Melzer C, de Boer B, van Duren JKJ, Janssen RAJ. Compositional dependence of the performance of poly(p-phenylene vinylene): methanofullerene bulk-heterojunction solar cells. *Advanced Functional Materials* 2005; **15**: 795–801.
49. Kim Y, Choulis SA, Nelson J, Bradley DDC, Cook S, Durrant JR. Device annealing effect in organic solar cells with blends of regioregular poly(3-hexylthiophene) and soluble fullerene. *Applied Physics Letters* 2005; **86**: 063502-1–063502-3.
50. Padinger F, Rittberger RS, Sariciftci NS. Effects of postproduction treatment on plastic solar cells. *Advanced Functional Materials* 2003; **13**: 85–88.
51. Al-Ibrahim M, Ambacher O, Sensfuss S, Gobsch G. Effects of solvent and annealing on the improved performance of solar cells based on poly(3-hexylthiophene): fullerene. *Applied Physics Letters* 2005; **86**: 201120-1–201120-3.
52. Reyes-Reyes M, Kim K, Carroll DL. High-efficiency photovoltaic devices based on annealed poly(3-hexylthiophene) and 1-(3-methoxycarbonyl)-propyl-1-

DOI: 10.1002/pip

phenyl-(6,6)C61 blends. *Applied Physics Letters* 2005; **87**: 083506-1–083506-3.
53. Li G, Shrotriya V, Yao Y, Yang Y. Investigation of annealing effects and film thickness dependence of polymer solar cells based on poly(3-hexylthiophene). *Journal of Applied Physics* 2005; **98**: 043704-1–043704-5.
54. Yamanari T, Taima T, Hara K, Saito K. Investigation of optimum conditions for high-efficiency organic thin-film solar cells based on polymer blends. *Journal of Photochemistry and Photobiology A: Chemistry* 2006; **182**: 269–272.
55. Yang X, Loos J, Veenstra SC, Verhees WJH, Wienk MM, Kroon JM, Michels MAJ, Janssen RAJ. Nanoscale morphology of high-performance polymer solar cells. *Nano Letters* 2005; **5**: 579–583.
56. Hoppe H, Sariciftci NS. Morphology of polymer/fullerene bulk heterojunction solar cells. *Journal of Materials Chemistry* 2006; **16**: 45–61.
57. Nakamura J, Murata K, Takahashi K. Relation between carrier mobility and cell performance in bulk heterojunction solar cells consisting of soluble polythiophene and fullerene derivatives. *Applied Physics Letters* 2005; **87**: 132105-1–132105-3.
58. Savenije TJ, Kroeze JE, Yang X, Loos J. The effect of thermal treatment on the morphology and charge carrier dynamics in a polythiophene-fullerene bulk heterojunction. *Advanced Functional Materials* 2005; **15**: 1260–1266.
59. Ma W, Yang C, Gong X, Lee K, Heeger AJ. Thermally stable, efficient polymer solar cells with nanoscale control of the interpenetrating network morphology. *Advanced Functional Materials* 2005; **15**: 1617–1622.
60. Douhéret O, Lutsen L, Swinnen A, Breselge M, Vandewal K, Goris L, Manca J. Nanoscale electrical characterization of organic photovoltaic blends by conductive atomic force microscopy. *Applied Physics Letters* 2006; **89**: 032107-1–032107-3.
61. Sliaužys G, Juška G, Arlauskas K, Pivrikas A, Österbacka R, Mozer A, Scharber M, Sarciftci NS. Recombination of photogenerated and injected charge carriers in pi-conjugated polymer/fullerene blends. *Thin Solid Films* 2006; **511**: 224–227.
62. Pivrikas A, Juška G, Arlauskas K, Scharber M, Mozer A, Sariciftci NS, Stubb H, Österbacka R. Charge carrier transport and recombination in bulk-heterojunction solar-cells. *Proceedings of SPIE* 2005; **5938**: 59380N-1–59380N-11.
63. Dennler G, Mozer AJ, Juška G, Pivrikas A, Österbacka R, Fuchsbauer DA, Sariciftci NS. Charge carrier mobility and lifetime versus composition of conjugated polymer/fullerene bulk-heterojunction solar cells. *Organic Electronics* 2006; **7**: 229–234.
64. Melzer C, Koop EJ, Mihailetchi VD, Blom PWM. Hole Transport in poly(phenylene vinylene)/methanofullerene bulk-heterojunction solar cells. *Advanced Functional Materials* 2004; **14**: 865–870.
65. Gommans HHP, Kemerink M, Kramer JM, Janssen RAJ. Field and temperature dependence of the photocurrent in polymer/fullerene bulk heterojunction solar cells. *Applied Physics Letters* 2005; **87**: 122104-1–122104-3.
66. Balberg I, Naidis R, Lee MK, Shinar J, Fonseca LF. Bipolar phototransport in pi-conjugated polymer/C60 composites. *Applied Physics Letters* 2001; **79**: 197–199.
67. Carius R, Becker F, Brüggemann R, Wagner H. Electroluminescence and forward bias currents in amorphous silicon p-i-n diodes: the effect of steady state bias and large i-layer thickness. *Journal of Non-Crystalline Solids* 1996; **198**: 246–250.
68. Vanderhaghen R, Han D. Interface effects on double injection current and photocurrent in a-Si:H n-i-p and p-i-n diodes. *Journal of Non-Crystalline Solids* 1996; **190**: 95–106.
69. Dean RH. Transient double injection in germanium. *Applied Physics Letters* 1968; **13**: 164–166.
70. Hack M, Street RA. Analysis of double injection transients in amorphous silicon p-i-n diodes. *Journal of Applied Physics* 1992; **72**: 2331–2339.
71. Dean RH. Transient double injection in semiconductors with traps. *Journal of Applied Physics* 1969; **40**: 596–602.
72. Dean RH. Transient double injection in trap-free semiconductors. *Journal of Applied Physics* 1969; **40**: 585–595.
73. Boon MR. Double injection into an intrinsic-conductor. *Thin Solid Films* 1972; **10**: 301–306.
74. Roberts GG, Tredgold RH. Double injection including diffusion effects. *Physics Letters* 1965; **14**: 94–95.
75. Juška G, Pivrikas A, Arlauskas K, Sliaužys G, Mozer AJ, Scharber M, Sariciftci NS, Österbacka R. Double injection as a technique to study charge carrier transport and recombination in bulk-heterojunction solar cells. *Applied Physics Letters* 2005; **87**: 222110-1–222110-3.
76. Juška G, Sliaužys G, Genevičius K, Arlauskas K, Pivrikas A, Scharber M, Dennler G, Sariciftci NS, Österbacka R. Charge-carrier transport and recombination in thin insulating films studied via extraction of injected plasma. *Physics Review B* 2006; **74**: 115314-1–115314-5.
77. Juška G, Sliaužys G, Genevičius K, Pivrikas A, Scharber M, Österbacka R. Double-injection current transients as a way of measuring transport in insulating organic films. *Journal of Applied Physics* 2007; **101**: 114505-1–114505-5.
78. Obarowska M, Godlewski J. Electric field dependence of the bimolecular recombination rate of the charge carriers. *Synthetic Metals* 2000; **109**: 219–222.
79. Chirvasea D, Chiguvare Z, Knipper M, Parisi J, Dyakonov V, Hummelen JC. Electrical and optical design and characterisation of regioregular poly(3-hexylthiophene-

DOI: 10.1002/pip

2,5diyl)/fullerene-based heterojunction polymer solar cells. *Synthetic Metals* 2003; **138**: 299–304.
80. Koster LJA, Mihailetchi VD, Xie H, Blom PWM. Origin of the light intensity dependence of the short-circuit current of polymer/fullerene solar cells. *Applied Physics Letters* 2005; **87**: 203502-1–203502-3.
81. von Hauff E, Parisi J, Dyakonov V. Field effect measurements on charge carrier mobilities in various polymer-fullerene blend compositions. *Thin Solid Films* 2006; **511**: 506–511.
82. Tuladhar SM, Poplavskyy D, Choulis SA, Durrant JR, Bradley DDC, Nelson J. Ambipolar charge transport in films of methanofullerene and poly(phenylenevinylene)/methanofullerene blends. *Advanced Functional Materials* 2005; **15**: 1171–1182.
83. Mihailetchi VD, van Duren JKJ, Blom PWM, Hummelen JC, Janssen RAJ, Kroon JM, Rispens MT, Verhees WJH, Wienk MM. Electron transport in a methanofullerene. *Advanced Functional Materials* 2003; **13**: 43–46.

DOI: 10.1002/pip